DALTON
FULL PAPER

Using pseudohalides (NCS^-, N_3^-) as a probe for the active site of (μ-alkoxo)diiron(III) complexes and to reveal a novel asymmetrical structure

Den-Nan Horng * and Kwang-Ming Lee

Department of Chemistry and Physics, The Chinese Military Academy, PO Box 90602-6, Fengshan, 830 Taiwan

Received 10th March 1999, Accepted 30 April 1999

A series of (μ-alkoxo)diiron(III) complexes $[Fe_2(L)Cl_4]Cl{\cdot}2H_2O$ **1**, $[Fe_2(L)(NCS)_n(Cl)_{4-n}]Cl{\cdot}\ 4H_2O$ **2–5** (n = 1–4) and $[Fe_2(L)(N_3)_n(Cl)_{4-n}]\ NO_3{\cdot}3H_2O$ **6–9** (n = 1–4), where HL is *N*,*N*,*N*′,*N*′-tetrakis(2-benzimidazolylmethyl)-2-hydroxy-1,3-diaminopropane, have been synthesized and their structures, magnetic and redox properties and Mössbauer spectra have been investigated. Three complexes **1**, **3** and **9** were characterized by single crystal structure analysis. The structures of **1** and **9** are geometrically symmetric, but **3** is asymmetric. The Mössbauer spectra of all complexes are typical of high-spin (μ-alkoxo)diiron(III) complexes. Complexes **2**–**9** exhibit intense IR bands (2022–2081 cm^{-1}) which are characteristic of terminally bound thiocyanate (N-bound) and azide ligands. The $E_{1/2}$ and the ΔE_{pc} of **1**, **3** and **9** increase with π-donor effectiveness of the exogenous ligands in the following order: $NCS^- < Cl^- < N_3^-$. The $-J$ (300−4.2 K) of **1**, **3** and **9** are in the range of 13.3–16.4 cm^{-1}, indicating that the iron(III) sites are antiferromagnetically coupled.

Introduction

The chemistry of dinuclear iron complexes is of particular importance to gain insight into the structures and functions of the active forms of proteins such as hemerythrin (Hr),[1,2] ribonucleotide reductase (RRB2)[3,4] and methane monooxygenase (MMO).[5–7] Dinuclear metal complexes with sterically and electronically controlled environments are expected to make different biofunctions. It is of interest not only to understand how these non-heme diiron proteins affect their respective chemical transformations but also to determine what factors direct the reactivity of their metallocenters to achieve a particular function.

It is often found that the dinuclear site of the metalloenzyme situates its metal ions in chemically distinct environments. From the perspective of the metal, four distinct environments can readily be identified:[8] (1) symmetric, (2) donor asymmetry, (3) geometrical asymmetry and (4) co-ordination number asymmetry. Many geometric symmetry or asymmetry model complexes have been reported, however the effects of changing from geometric symmetry into asymmetry on the physical properties and function of dinuclear sites are much less studied.

Pseudohalides, such as thiocyanate and azide ions, can be used as probes for the active-site structures of non-heme diiron proteins. For example, crystallographic investigations revealed that the binding modes of azidomethemerythrin and oxyhemerythrin (oxyHr) are almost identical.[9,10] Recent examples of azide adducts[11] have also been reported. Nevertheless, only two crystal structures of thiocyanate-bound diiron model compounds had been published so far.[12,13]

Our interest in the active sites of dinuclear iron proteins has led us to the exploration of pseudohalide-bound diiron(III) complexes and to study the influence of pseudohalides, such as thiocyanate and azide ions, on the structure of (μ-alkoxo)diiron(III) complexes of HL (*N*,*N*,*N*′,*N*′-tetrakis(2-benzimidazolylmethyl)-2-hydroxy-1,3-diaminopropane). The bis-octahedral $[Fe_2(L)X_4]^+$ complexes comprise two five-membered rings involving 2-hydroxypropane chains and four five-membered rings resulting from the co-ordination of the (benzimidazolylmethyl)amino fragments of the polydentate ligand. Scheme 1

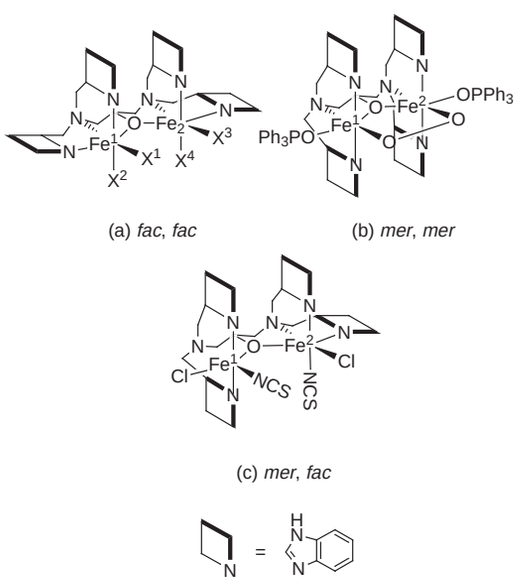

Scheme 1 Three possible conformations of $[Fe_2(L)X_4]^+$.

shows three possible isomer structures for $[Fe_2(L)X_4]^+$; the two pairs of benzimidazole rings of the ligand can have three possible arrangements, such as facial–facial, meridional–meridional and meridional–facial forms. We have synthesized a series of diiron complexes $[Fe_2(L)(X)_n(Cl)_{4-n}]Cl$ (X = NCS^- or N_3^-, n = 0–4) and three crystal structures were determined. It is interesting that $[Fe_2(L)Cl_4]Cl{\cdot}2H_2O$ and $[Fe_2(L)(N_3)_4]NO_3{\cdot}3H_2O$ are *mer*, *mer* geometrically symmetric structures, but $[Fe_2(L)(NCS)_2Cl_2]Cl{\cdot}4H_2O$ is a *fac*, *mer* asymmetric one. To our best knowledge, this is the first example that pseudohalide can induce asymmetric geometry from symmetric. In this paper we report the characterization of the complexes by single crystal X-ray diffraction, magnetic susceptibility, Mössbauer, redox

and optical spectroscopic techniques and explore the influence of pseudohalide on geometric symmetry.

Experimental

1,2-Diaminobenzene was sublimed before use, while all other chemicals were A.R. grade used without further purification.

Preparations

***N*,*N*,*N*′,*N*′-Tetrakis(2-benzimidazolylmethyl)-2-hydroxy-1,3-diaminopropane trihydrate HL·3H$_2$O.** The ligand, HL was synthesized by condensing 1,2-diaminobenzene with 2-hydroxy-1,3-diaminopropane-*N*,*N*,*N*′,*N*′-tetraacetic acid, utilizing the procedure reported earlier by Reed and co-workers.[14] It was characterized by ^{1}H NMR in DMSO-d$_6$ (Calc. for $C_{35}H_{40}N_{10}O_4$: C, 63.24; H, 6.06; N, 21.07. Found: C, 63.15; H, 6.01; N, 20.98%).

[Fe$_2$(L)Cl$_4$]Cl·2H$_2$O 1. Iron(III) chloride (0.324 g, 2 mmol) and HL (0.665, 1 mmol) were mixed in 50 ml EtOH and stirred for 10 min. After standing for about 1 d, the dark orange solution yielded red rhombic crystals. The crystals were suitable for single-crystal structure analysis. Yield 0.81 g (85%) (Calc. for $C_{35}H_{37}Cl_5Fe_2N_{10}O_3$: C, 45.06; H, 4.00; N, 15.02. Found: C, 43.88; H, 4.01; N, 14.58%).

[Fe$_2$(L)(NCS)$_n$(Cl)$_{4-n}$]Cl·4H$_2$O 2–5 (n = 1–4). A solution of complex **1** (0.191 g, 0.2 mmol) in 50 ml methanol was treated with $n \times 0.2$ mmol of $AgNO_3$. After stirring overnight, the white precipitate of AgCl was removed by filtration and the solution mixed with $n \times 0.1$ mmol of KSCN in 20 ml methanol. The resulting red-wine solution was allowed to crystallize at room temperature for about 2 d, yielding wine-colored microcrystals (72–80% yield). Only the crystals of **3** were suitable for single-crystal structure analysis [Calc. for $C_{36}H_{41}Cl_4Fe_2N_{11}O_5S$ **2**: C, 43.53; H, 4.16; N, 15.51. Found: C, 43.30; H, 4.08; N, 15.42%. ν_{CN} 2031 cm^{-1} (KBr pellet). Calc. for $C_{37}H_{41}Cl_3Fe_2N_{12}O_5S_2$ **3**: C, 43.74; H, 4.07; N, 16.54. Found: C, 43.48; H, 3.95; N, 16.37%. ν_{CN} 2023 cm^{-1}. Calc. for $C_{38}H_{41}Cl_2Fe_2N_{13}O_5S_3$ **4**: C, 43.95; H, 3.98; N, 17.53. Found: C, 43.88; H, 3.88; N, 17.38%. ν_{CN} 2023 cm^{-1}. Calc. for $C_{39}H_{41}ClFe_2N_{14}O_5S_4$ **5**: C, 44.14; H, 3.89; N, 18.48. Found: C, 44.12; H, 3.75; N, 18.32%. ν_{CN} 2022 cm^{-1}].

[Fe$_2$(L)(N$_3$)$_n$(Cl)$_{4-n}$]NO$_3$·3H$_2$O 6–9 (n = 1–4). The preparative procedure is almost identical with that described above, except that KSCN was replaced by NaN_3. Only the crystals of **9** were suitable for single-crystal structure analysis (Calc. for $C_{35}H_{39}Cl_3Fe_2N_{14}O_7$ **6**: C, 42.64; H, 3.99; N, 19.89. Found: C, 41.02; H, 3.90; N, 19.05%. ν_{NN} 2076 cm^{-1}. Calc. for $C_{35}H_{39}Cl_2Fe_2N_{17}O_7$ **7**: C, 42.36; H, 3.96; N, 23.99. Found: C, 41.48; H, 3.87; N, 22.87%. ν_{CN} 2081 cm^{-1}. Calc. for $C_{35}H_{39}ClFe_2N_{20}O_7$ **8**: C, 42.08; H, 3.94; N, 28.04. Found: C, 41.78; H, 4.01; N, 27.58%. ν_{CN} 2081 cm^{-1}. Calc. for $C_{35}H_{39}Fe_2N_{23}O_7$ **9**: C, 41.81; H, 3.91; N, 32.04. Found: C, 41.82; H, 3.80; N, 31.62%. ν_{CN} 2051 and 2077 cm^{-1}).

Physical measurements

Elemental analyses: Heraeus CHN-O-Rapid Analyzer. ^{1}H NMR: Bruker AC300 spectrometer at 300 MHz. Infrared spectrum: Perkin-Elmer FT-IR spectrometer using KBr pellets. Electronic spectra: Shimadzu UV-210 spectrometer at room temperature in MeOH. Cyclic voltammetry: BAS-100A Electrochemical Analyzer using a three-compartment cell. A platinum working electrode, platinum-wire auxiliary and a Ag–Ag$^+$ (0.01 mmol dm^{-3} $AgNO_3$ in CH_3CN–DMSO 10:1) reference electrode were employed. All solutions were degassed by purging with nitrogen for at least 15 min prior to use. The ferrocene–ferrocenium couple was employed as an internal reference. The magnetic susceptibility of a polycrystalline sample was measured by using a Quantum Design SQUID susceptometer. The sample was loaded anaerobically into a gel capsule and suspended in a plastic straw. A background correction for the empty capsule and straw was applied to the data; a total of 31 data points were collected in the temperature range 4.2 to 300 K. ^{57}Fe Mössbauer measurements were made on a constant-velocity instrument, previously described.[15] Velocity calibration was made using a 10 mg 99.99% pure iron foil. Typical linewidths for all three pairs of iron foil lines fell in the range 0.24–0.27 mm s^{-1}. Isomer shifts are reported relative to iron foil at 300 K.

Crystal structure determination

Single crystals of complexes **1**, **3** and **9** were obtained by vapor diffusion of diethyl ether into concentrated ethanol solutions of the respective complexes. The crystal data of **1** and **9** were collected on a Enraf-Nonius CAD4 four-circle diffractometer equipped with a graphite monochromator using Mo-Kα radiation (λ = 0.71073 Å). The data of **3** were collected on a Siemens P4 diffractometer equipped with a graphite monochromator using Mo-Kα radiation. Details of crystal parameters, data collection and structure refinement are summarized in Table 1. The structures were solved by the direct method using SHELXTL PLUS[16] and refined using SHELXL 93.[17] All non-hydrogen atoms, except for some belonging to the solvent molecules, were refined anisotropically. All H atoms, except for water, at calculated positions with thermal parameters equal to 1.2 times that of the attached C atoms were not refined. The counter anion chloride of **3** and the water of complexes **3** and **9** are disordered over several positions, to which some restraints were applied and modeled using different molecules with occupancies of 0.15–0.5.

CCDC reference number 186/1448.

See http://www.rsc.org/suppdata/dt/1999/2205/ for crystallographic files in .cif format.

Results and discussion

The ligand HL, which has four benzimidazole fragments, is known to act as a bridge in diiron(III) complexes and has proven to be suitable for the synthesis of dinuclear metal complexes.[18–25] The syntheses of [Fe$_2$(L)(X)$_n$(Cl)$_{4-n}$]Cl·3H$_2$O complexes with X$^-$ = NCS$^-$ or N_3^- proceed in excellent yield, chloride being displaced from Fe$_2$(L)(Cl)$_{5-n}$(NO$_3$)$_n$ by pseudohalide nucleophiles. The presence of NCS$^-$ (N-bonded) or N_3^- ligands in complexes **2**–**9** is indicated by sharp CN or NN stretches between 2030 and 2070 cm^{-1}.

Reaction of 2 molar equivalents of $FeCl_3$ in ethanol with one of HL leads to red crystals of [Fe$_2$(L)Cl$_4$]Cl·2H$_2$O **1**. In an earlier study, Sakurai *et al.*[18] reported a diiron(III) complex Fe$_2$(L)Cl$_5$ and a μ-alkoxo diiron core structure capped by the L ligand and four chloro ligands was proposed. The structure of complex **1** agrees with the proposed structure. The complex [Fe$_2$(L)Cl$_4$]Cl·2H$_2$O crystallized in the monoclinic space group *C*2/*c*. An ORTEP[26] drawing of the cation is shown Fig. 1(a), and selected interatomic distances and angles are listed in Table 2. The structure reveals that the iron(III) ions in the dinuclear complex are six-co-ordinated in a distorted octahedral geometry. Each metal atom has two benzimidazole moieties, a tertiary nitrogen atom, a bridging alkoxo oxygen atom and two chloro ligands. The Fe···Fe separation of 3.712(5) Å, similar to those found in related complexes which do not have bridging ligands,[21] but larger than that found in complexes having bridged ligands, for example [Fe$_4$O$_2$(L)$_2$(O$_2$CPh)$_2$][ClO$_4$]$_2$-[O$_3$SC$_6$H$_4$Me-*p*]$_2$ and [Fe$_4$O$_2$(L′)$_2$(OAc)$_2$][BF$_4$]$_4$,[22] (L′ is the 1-ethylbenzimidazole derivative of L) that exhibit Fe···Fe distances between 3.539 and 3.488(2) Å in their carboxylato bridged Fe$_2$ units. Each iron core has two benzimidazole ligands co-ordinated *cis* to each other (*fac* form), with two ring planes

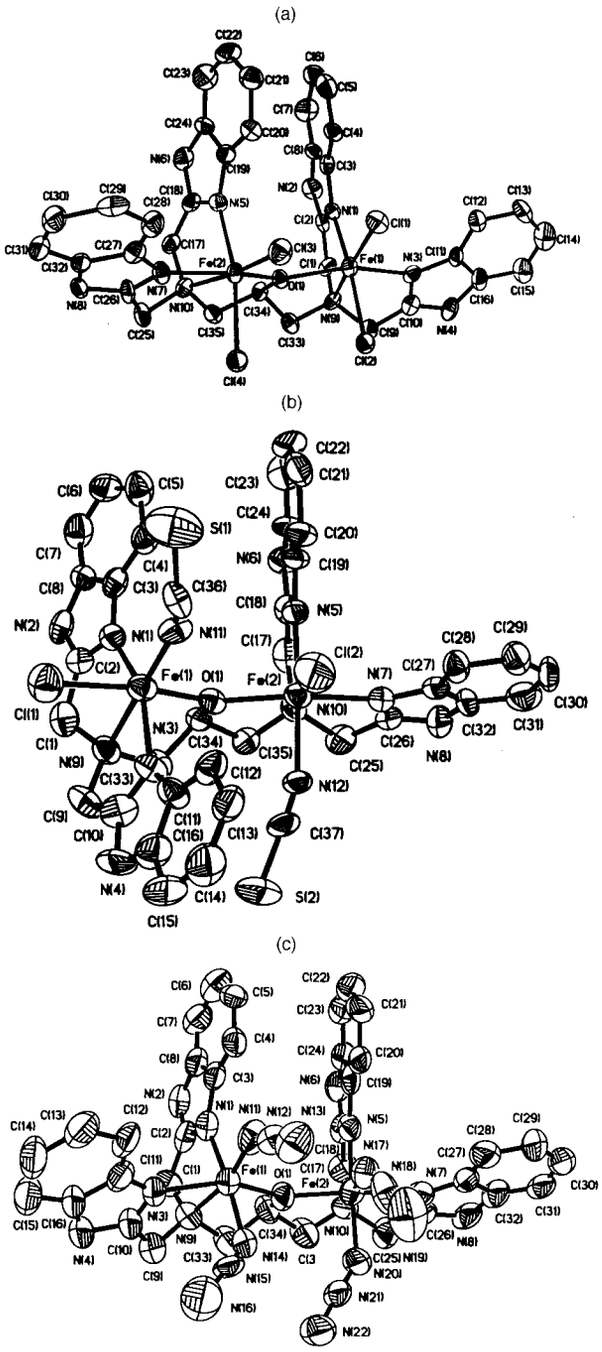

Fig. 1 The crystal structures of the complex cations of complexes **1** (a), **3** (b) and **9** (c). Thermal ellipsoids are at the 30% probability level. Hydrogen atoms are omitted for clarity.

perpendicular to each other (85–90°). One benzimidazole ligand is co-ordinated *trans* to a chloride and another *trans* to an alkoxide ligand. The co-ordination sphere is completed by a chloride and tertiary amine ligands in *trans* position. The Fe–Cl bond length is affected by *trans* influence; those *trans* to tertiary amine (2.207(4) and 2.226(4) Å) are shorter than those *trans* to benzimidazole (2.391(4) and 2.352(4) Å).

Treatment of complex **1** with two equivalents of KNCS yields $[Fe_2(L)(NCS)_2Cl_2]Cl{\cdot}4H_2O$ **3**, in which two chloro ligands (in **1**) have been displaced by two thiocyanate ligands. Most of the known related compounds have two of the benzimidazoles bound to an iron atom in a *cis* fashion (Scheme 1(a), *fac*, *fac* form). Only one structurally characterized iron(III) complex has been found to have two benzimidazoles bound to one iron atom in a *trans* form (Scheme 1(b), *mer*, *mer* form). To our best knowledge, no example has been found where L is bound in an asymmetric manner (Scheme 1(c), *mer*, *fac* form). The molecular structure of **3** is depicted in Fig. 1(b), and selected interatomic distances and angles are listed in Table 3. When compared with **1**, each iron atom has one chloride replaced by one thiocyanate ligand. It is interesting that the two iron centers have the same N_4OCl co-ordination sphere, but different co-ordination mode. For the Fe1 center the two benzimidazole ligands are co-ordinated *cis* to each other and one thiocyanate is *trans* to N5(benzimidazole). At Fe2, the two benzimidazole ligands co-ordinate *trans* to each other and the two benzimidazole rings are perpendicular to the plane defined by the two iron atoms and the alkoxide; the thiocyanate ligands are *trans* to the tertiary amine(N10). Complex **3**, therefore, is not only one of the three known examples having a terminal thiocyanate co-ordinated at an iron(III) center, but also the first example of a dinuclear iron(III) complex having asymmetrically bonded benzimidazole moieties in a *mer*, *fac* form. The co-ordination sphere around the Fe2 center is similar to that of $[Fe_2(L)Cl_4]Cl$, while that of Fe1 is similar to that of $[Fe_2(\mu\text{-}1,2\text{-}O_2)(L')(Ph_3PO)_2]$ reported by Que and co-workers.[24] Especially, the mean Fe1–N (benzimidazole) distance of 2.078(13) Å is similar to that of $[Fe_2(\mu\text{-}1,2\text{-}O_2)(L')(Ph_3PO)_2]$ (2.088(4) Å). The structural similarity between the co-ordination spheres of Fe1 and that of the O_2 adduct in the non-heme diiron complex $[Fe_2(\mu\text{-}1,2\text{-}O_2)(L')(Ph_3PO)_2]$ suggests that NCS indeed is a good ligand to probe the active site of non-heme diiron proteins. The asymmetrical structure of **3** has two interesting features as compared with that of **1** and $[Fe_2(\mu\text{-}1,2\text{-}O_2)(L')(Ph_3PO)_2]$. First, the conformations of the two irons are independent, although L is a symmetrical ligand. This property is similar to that of diiron proteins such as hemerythrin. Secondly, the co-ordination sites of the two irons are distinct; only when the iron center bonds to one thiocyanate which is *trans* to a tertiary amine, the two benzimidazoles are in a *trans* form.

The azide adduct $[Fe_2(L)(N_3)_4]NO_3{\cdot}3H_2O$ **9** crystallized in the monoclinic space group *C*2/*c*. An ORTEP drawing of the structure is shown in Fig. 1(c), and selected interatomic distances and angles are listed in Table 4. A general feature of **9** is that its structural parameters are similar but not identical with those of **1**, two pairs of benzimidazoles also bound to each iron atom in a *cis* form. Table 5 compares the partial structural parameters of **1**, **3** and **9** with those of related (μ-alkoxo)-diiron(III) complexes. Complex **10**, $[Fe_2(L)\{O_2P(OPh)_2\}Cl_2(MeOH)]^{2+}$, is a mono-bridged complex of the μ-alkoxo variety, $[Fe_4O_2(L')_2(OAc)_2]^{4+}$ **11**;[22] $[Fe_2(L)(O_2AsMe_2)Cl(H_2O)]^{3+}$ **12**;[23] $[Fe_2(\mu\text{-}1,2\text{-}O_2)(L')(PH_3PO)_2]^{3+}$ **13**;[24] and $[Fe_2(NO)_2(L')(O_2C\text{-}Ph)]^{2+}$ **14**[25] are dibridged complexes. A general feature of the monobridged species is that their structural parameters are different from those of dibridged ones. Thus, **1**, **3** and **10** have longer Fe···Fe distances (3.700(2)–3.717(6) Å) and larger Fe–O–Fe angles (130.9(2)–132.0(4)°) than the others. It is noticeable that the Fe–O–Fe angle of **9** (127.9(5)°) is the smallest among those of other monobridged complexes. The alkoxo-bridge in **9** constrains the Fe···Fe distance to 3.642 Å. These values are comparable to those found for the dibridged complex **12**. The two other dibridged complexes **11** and **13** have somewhat shorter Fe···Fe distances (3.49 and 3.46 Å) and smaller Fe–O–Fe angles (120.9, 120.8°). It is interesting that both the azide adduct **9** and the dioxygen adduct **13** have longer Fe–N (tertiary) bond distances (2.315(11) for **9**, 2.364(5) for **13**, 2.25–2.30 Å for the other complexes), which can be explained by the *trans* influence of azide on tertiary amine. The Fe-N (benzimidazole) distances (2.049(12)–2.154(10) Å) of **1**, **3** and **9** also fall in the range found in **10**–**14** (2.06–2.23 Å).

Cyclic voltammetry

Cyclic voltammograms of these complexes were recorded in a mixed-solvent system (CH_3CN–DMSO 10:1) owing to the insolubility of the compounds in CH_3CN. The redox processes are in a region (−0.7 to +0.2 V) free from solvent interference.

Table 1 Crystallographic data for complexes **1**, **3** and **9**

	1	**3**	**9**
Chemical formula	$C_{35}H_{37}Cl_5Fe_2N_{10}O_3$	$C_{37}H_{41}Cl_3Fe_2N_{12}O_5S_2$	$C_{35}H_{39}Fe_2N_{23}O_7$
M	934.70	1015.99	1005.59
Crystal system	Monoclinic	Monoclinic	Monoclinic
Space group	$C2/c$	$P2_1/c$	$C2/c$
a/Å	22.365(3)	13.638(3)	21.338(4)
b/Å	13.812(2)	22.508(3)	15.685(3)
c/Å	28.778(4)	17.667(3)	28.017(6)
β/°	105.05(1)	99.56(2)	102.68(3)
V/Å^3	8585(2)	5348(2)	9148(3)
Z	8	4	8
T/K	293(2)	293(2)	293(2)
D_c/g cm^{-3}	1.446	1.262	1.460
$F(000)$	3824	2088	4144
μ/mm^{-1}	1.033	0.817	0.707
Reflections collected/unique (R_{int})	5552	7271/6933(0.0566)	9175/8980(0.0875)
Data/restraints/parameters	5552/0/487	6930/21/576	8971/20/612
Final $R1$, $wR2$ [$I > 2\sigma(I)$]	0.0744, 0.1990	0.0894, 0.2420	0.0828, 0.1944
Largest difference peak and hole/e Å^{-3}	1.176, −0.495	0.587, −0.482	0.623, −0.373

Table 2 Selected bond lengths (Å) and angles (°) for $[Fe_2(L)Cl_4]^+$

Fe(1)···Fe(2)	3.712(5)	Fe(1)–O(1)	2.043(8)
Fe(2)–O(1)	2.021(8)	Fe(1)–N(1)	2.122(10)
Fe(1)–N(3)	2.154(10)	Fe(1)–N(9)	2.279(10)
Fe(1)–Cl(1)	2.226(4)	Fe(1)–Cl(2)	2.352(4)
Fe(2)–N(5)	2.108(11)	Fe(2)–N(7)	2.119(10)
Fe(2)–N(10)	2.257(10)	Fe(2)–Cl(3)	2.207(4)
Fe(2)–Cl(4)	2.391(4)		
Fe(1)–O(1)–Fe(2)	132.0(4)	O(1)–Fe(1)–N(1)	89.1(3)
O(1)–Fe(1)–N(3)	154.3(4)	O(1)–Fe(1)–N(9)	81.2(3)
O(1)–Fe(1)–Cl(1)	107.7(3)	O(1)–Fe(1)–Cl(2)	88.7(2)
N(1)–Fe(1)–N(3)	89.5(4)	N(1)–Fe(1)–N(9)	77.8(4)
N(1)–Fe(1)–Cl(1)	95.4(3)	N(1)–Fe(1)–Cl(2)	166.5(3)
N(3)–Fe(1)–N(9)	73.4(4)	N(3)–Fe(1)–Cl(1)	98.0(3)
N(3)–Fe(1)–Cl(2)	86.6(3)	N(9)–Fe(1)–Cl(1)	169.0(3)
N(9)–Fe(1)–Cl(2)	88.7(3)	Cl(1)–Fe(1)–Cl(2)	97.92(14)
O(1)–Fe(2)–N(5)	89.3(3)	O(1)–Fe(2)–N(7)	152.7(4)
O(1)–Fe(2)–N(10)	78.9(3)	O(1)–Fe(2)–Cl(3)	107.8(3)
O(1)–Fe(2)–Cl(4)	93.0(2)	N(5)–Fe(2)–N(7)	84.7(4)
N(5)–Fe(2)–N(10)	78.4(4)	N(5)–Fe(2)–Cl(3)	97.8(3)
N(5)–Fe(2)–Cl(4)	166.8(3)	N(7)–Fe(2)–N(10)	73.7(4)
N(7)–Fe(2)–Cl(3)	99.4(3)	N(7)–Fe(2)–Cl(4)	87.3(3)
N(10)–Fe(2)–Cl(3)	172.3(3)	N(10)–Fe(2)–Cl(4)	89.3(3)
Cl(3)–Fe(2)–Cl(4)	93.9(2)		

Table 3 Selected bond lengths (Å) and angles (°) for $[Fe_2(L)(NCS)_2Cl_2]^+$

Fe(1)···Fe(2)	3.717(6)	Fe(1)–O(1)	2.005(9)
Fe(2)–O(1)	2.065(9)	Fe(1)–N(1)	2.068(12)
Fe(1)–N(3)	2.087(13)	Fe(1)–N(9)	2.257(12)
Fe(1)–Cl(1)	2.382(5)	Fe(1)–N(11)	1.920(13)
Fe(2)–N(5)	2.142(11)	Fe(2)–N(7)	2.109(12)
Fe(2)–N(10)	2.257(11)	Fe(2)–N(12)	2.045(13)
Fe(2)–Cl(2)	2.220(8)		
Fe(1)–O(1)–Fe(2)	131.9(4)	O(1)–Fe(1)–N(1)	89.0(4)
O(1)–Fe(1)–N(3)	92.4(4)	O(1)–Fe(1)–N(9)	81.5(4)
O(1)–Fe(1)–Cl(1)	168.4(3)	O(1)–Fe(1)–N(11)	98.1(6)
N(1)–Fe(1)–N(3)	154.1(6)	N(1)–Fe(1)–N(9)	77.3(5)
N(1)–Fe(1)–Cl(1)	87.0(3)	N(1)–Fe(1)–N(11)	101.8(6)
N(3)–Fe(1)–N(9)	77.3(5)	N(3)–Fe(1)–Cl(1)	86.6(4)
N(3)–Fe(1)–N(11)	103.6(6)	N(9)–Fe(1)–Cl(1)	87.0(4)
N(9)–Fe(1)–N(11)	179.0(6)	Cl(1)–Fe(1)–N(11)	93.4(5)
O(1)–Fe(2)–N(5)	89.0(4)	O(1)–Fe(2)–N(7)	154.3(5)
O(1)–Fe(2)–N(10)	79.1(4)	O(1)–Fe(2)–Cl(2)	108.1(3)
O(1)–Fe(2)–N(12)	87.2(4)	N(5)–Fe(2)–N(7)	88.5(4)
N(5)–Fe(2)–N(10)	79.0(5)	N(5)–Fe(2)–Cl(2)	95.4(4)
N(5)–Fe(2)–N(12)	167.5(6)	N(7)–Fe(2)–N(10)	75.4(5)
N(7)–Fe(2)–Cl(2)	97.6(5)	N(7)–Fe(2)–N(12)	89.8(5)
N(10)–Fe(2)–Cl(2)	170.9(4)	N(10)–Fe(2)–N(12)	88.6(5)
Cl(2)–Fe(2)–N(12)	97.1(4)		

Table 4 Selected bond lengths (Å) and angles (°) for $[Fe_2(L)(N_3)_4]^+$

Fe(1)···Fe(2)	3.642(6)	Fe(1)–O(1)	2.039(7)
Fe(2)–O(1)	2.014(7)	Fe(1)–N(1)	2.068(12)
Fe(1)–N(3)	2.106(10)	Fe(1)–N(9)	2.315(11)
Fe(1)–N(11)	1.893(13)	Fe(1)–N(14)	2.01(2)
Fe(2)–N(5)	2.049(12)	Fe(2)–N(7)	2.103(10)
Fe(2)–N(10)	2.255(12)	Fe(2)–N(17)	1.838(14)
Fe(2)–N(20)	1.996(13)		
Fe(1)–O(1)–Fe(2)	127.9(5)	O(1)–Fe(1)–N(1)	92.3(4)
O(1)–Fe(1)–N(3)	152.1(5)	O(1)–Fe(1)–N(9)	79.1(4)
O(1)–Fe(1)–N(11)	107.3(5)	O(1)–Fe(1)–N(14)	88.5(5)
N(1)–Fe(1)–N(3)	90.3(4)	N(1)–Fe(1)–N(9)	76.4(6)
N(1)–Fe(1)–N(11)	90.4(6)	N(1)–Fe(1)–N(14)	174.4(7)
N(3)–Fe(1)–N(9)	74.6(5)	N(3)–Fe(1)–N(11)	100.5(6)
N(3)–Fe(1)–N(14)	86.4(5)	N(9)–Fe(1)–N(11)	165.7(5)
N(9)–Fe(1)–N(14)	98.3(7)	N(11)–Fe(1)–N(14)	94.7(7)
O(1)–Fe(2)–N(5)	88.7(3)	O(1)–Fe(2)–N(7)	153.1(5)
O(1)–Fe(2)–N(10)	78.1(4)	O(1)–Fe(2)–N(17)	108.0(5)
O(1)–Fe(2)–N(20)	91.8(4)	N(5)–Fe(2)–N(7)	85.7(3)
N(5)–Fe(2)–N(10)	78.1(5)	N(5)–Fe(2)–N(17)	96.9(6)
N(5)–Fe(2)–N(20)	165.7(6)	N(7)–Fe(2)–N(10)	75.0(5)
N(7)–Fe(2)–N(17)	98.8(5)	N(7)–Fe(2)–N(20)	87.5(4)
N(10)–Fe(2)–N(17)	172.3(5)	N(10)–Fe(2)–N(20)	87.9(5)
N(17)–Fe(2)–N(20)	96.6(6)		

Ferrocene was used as internal standard, yielding the Fc–Fc$^+$, one-electron couple at $E_m = 0.2$ V *vs.* Ag–Ag+.

The cyclic voltammograms of complexes **1**, **3** and **9** are shown in Fig. 2. Complex **1** exhibits an irreversible reduction at −0.51 V and a coupled oxidation–reduction wave at −0.218 and −0.345 V, respectively. The $E_{1/2}$ value for this process is −0.282 V, however, ΔE is 0.12 V. The redox process therefore by definition is quasi-reversible.[27] The voltammograms of complexes **3** and **9** are displayed in Fig. 2(b) and 2(c). Two quasi-reversible redox processes are observed for each complex corresponding to successive one-electron-transfer steps. The redox steps at −0.227 and −0.423 V for **3** and at −0.356 and −0.508 V for **9** correspond to the $Fe^{III}Fe^{III}$–$Fe^{II}Fe^{III}$ and $Fe^{II}Fe^{III}$–$Fe^{II}Fe^{II}$ couples, respectively.

The HOMO level has the correct symmetry to interact with benzimidazole π* orbitals and p_π-donor orbitals of halide and pseudohalide ligands. The $E_{1/2}$ of complexes **1**, **3** and **9** are −0.282, −0.227 and −0.356 V and the ΔE_{pc} of complexes **1**, **3** and **9** are −0.160, −0.169 and −0.145 V. Both increase with π-donor effectiveness of the exogenous ligands,[28] in the following order: $NCS^- < Cl^- < N_3^-$.

Mössbauer spectrum

The Mössbauer spectra for complexes **1**, **3** and **9** were recorded

Table 5 Comparison of relevant distances, angles and physical properties for (μ-alkoxo)diiron(III) complexes

Feature	1	3	9	10	11	12	13	14
Fe···Fe	3.712(5)	3.717(6)	3.642(6)	3.700(2)	3.488(2)	3.580(2)	3.462(3)	[a]
Fe–O–Fe	132.0(4)	131.9(4)	127.9(5)	130.9(2)	120.9(4)	127.3(3)	120.8(3)	117.7(2)
Fe–O	2.043(8)	2.005(9)	2.039(7)	2.011(4)	1.995(2)	1.971(6)	1.991(3)	2.017(5)
	2.021(8)	2.065(9)	2.014(7)	2.056(4)	2.018(2)	2.025(6)	1.991(3)	2.006(5)
Fe–N(3°)[b]	2.279(10)	2.257(12)	2.315(11)	2.295(4)	2.25(1)	2.288(7)	2.364(5)	2.290(6)
	2.257(10)	2.257(11)	2.255(12)	2.276(4)	2.26(1)	2.269(7)	2.364(5)	2.282(7)
Fe–N(Bim)[c]	2.122(10)	2.068(12)	2.068(12)	2.120(5)	2.22(1)	2.063(7)	2.082(4)	2.119(7)
	2.154(10)	2.087(13)	2.106(10)	2.106(4)	2.16(1)	2.086(7)	2.094(4)	2.117(7)
	2.108(11)	2.142(11)	2.049(12)	2.138(5)	2.23(1)	2.077(8)	2.082(4)	2.114(7)
	2.119(10)	2.109(12)	2.103(10)	2.073(4)	2.16(1)	2.055(7)	2.094(4)	2.135(7)
$-J$/cm^{-1}	13.3	16.4	15.1	13.7	83	10.3	[a]	23
δ/mm s^{-1}	0.36	0.35	0.37	0.46	[a]	0.35, 0.35	0.52	0.67
ΔE_Q/mm s^{-1}	0.54	0.51	0.58	0.59	[a]	0.37, 0.65	0.72	1.44
Ref.	This work	This work	This work	21	22	23	24	25

[a] Not reported. [b] N(3°) refers to the tertiary amine nitrogen. [c] N(Bim) refers to the benzimidazole nitrogen.

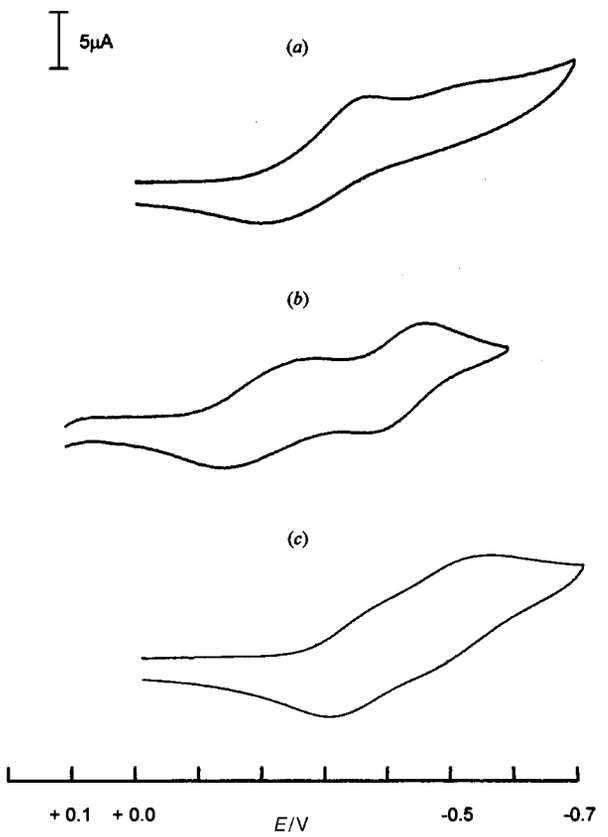

Fig. 2 Cyclic voltammograms of complexes **1** (*a*), **3** (*b*) and **9** (*c*), scan rate 0.5 V s^{-1}.

at room temperature and all show a slight asymmetrical quadruple doublet. The isomer shifts (δ) and quadruple splitting (ΔE_Q) are summarized in Table 5. Since the isomer shifts for high-spin mononuclear and alkoxo-bridged binuclear iron(III) complexes generally fall in the range 0.3–0.6 mm s^{-1},[29] the present isomer shifts (0.35–0.37 mm s^{-1}) are consistent with the presence of high-spin iron(III) ions.

Magnetic susceptibility

The magnetic susceptibility of complexes **1**, **3** and **9** were measured in the temperature range 4.2 to 300.0 K, and the coupling constants found are listed in Table 5. Fig. 3 shows the experimental data and fitted curves of magnetic susceptibility of **3**. The magnetic moment at room temperature is 3.88 μ_B. With lowering of the temperature the magnetic moment decreases and reaches 0.13 μ_B at 4.2 K. This magnetic behavior suggested the operation of an antiferromagnetic spin exchange. The

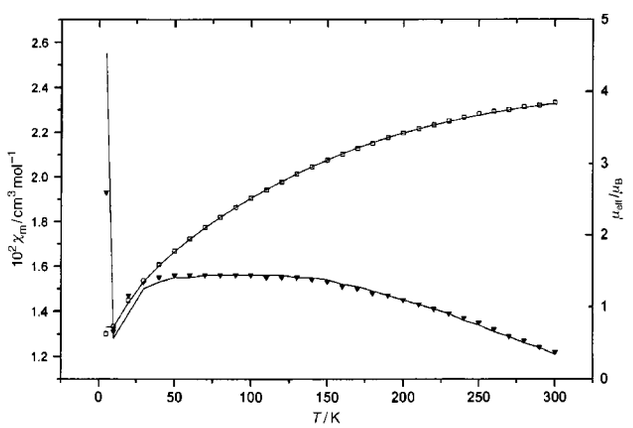

Fig. 3 The experimental data and fitted curves of magnetic susceptibility (▼) and moments (□) of complex **3**.

magnetic data could be fitted on the basis of an isotropic Heisenberg model $H' = -2JS_1S_2$ ($S_1 = S_2 = 5/2$), eqn. (1), where

$$\chi_m = C(1 - P)\cdot\frac{A}{B} + 4.37\frac{2p}{T} + \text{t.i.p.} \qquad (1)$$

$A = 2e^{2x} + 10e^{6x} + 28e^{12x} + 60e^{20x} + 110e^{30x}$, $B = 1 + 3e^{2x} + 5e^{6x} + 7e^{12x} + 9e^{20x} + 11e^{30x}$, $C = N\beta^2g^2/kT$ and $x = J/kT$. The symbols N, β, g and k in these expressions have their usual meanings, and p represents the fraction of mononuclear paramagnetic impurity present. The shapes of the plots in Fig. 3 are clearly indicative of antiferromagnetic exchange interactions. All the three diiron(III) complexes **1**, **3** and **9** are weakly antiferromagnetic, the $-J$ values decreasing in the order **3** (16.4) > **9** (15.1) > **1** (13.3 cm^{-1}). This order is consistent with the magnetostructural relationship proposed by Gorun and Lippard.[30] These values are in the typical range for μ-alkoxo or μ-hydroxo bridged systems.

Electronic spectroscopy

Electronic absorption spectra in the UV-visible region of **1**, **3** and **9** complexes were recorded in methanol solution and the data are collected in Table 6. The absorption bands below 300 nm are due to "free" ligand, and their absorption coefficients are typical of $\pi \longrightarrow \pi^*$ transitions. Complex **1** exhibits intense UV bands in MeOH but no significant visible absorption. Complex **3** shows a more intense peak at 480 nm (ε_m 4816 M^{-1} cm^{-1}), while this region of **1** is featureless. Complex **9** show a peak at 342 nm (ε_m 4291 M^{-1} cm^{-1}) with a less intense shoulder at about 450 nm. These two bands of **3** and **9** originate from N(N$_3$) and N(NCS) to iron charge transfer and give information on the energy separation between the ground and excited

Table 6 Quantitative spectral data of complexes **1**, **3** and **9**

Complex	λ_{max}/nm	ε/M^{-1} cm^{-1}
1	239	13040
	272	15760
	278	15328
	333	3136
3	243	16208
	272	17088
	279	16880
	331	3120
	480	4816
9	242	15439
	272	16566
	279	16087
	342	4291

states. In the crystal structure of **9**, the four N_3^- have N–N–N angles in the range of 173–178°. Bent N_3^- bound to Fe^{III} will have two allowed LMCT transitions.[31] This is also consistent with the CV measurement, in that the reduction potential E_{pc}(**3**) is more positive than E_{pc}(**9**).

Acknowledgements

Research grants from the National Science Council of Taiwan and The Chinese Military Academy are highly appreciated.

References

1 R. E. Stenkamp, *Chem. Rev.*, 1994, **94**, 715.
2 M. A. Holmes, I. L. Trong, S. Turley, L. C. Sieker and R. E. Stenkamp, *J. Mol. Biol.*, 1991, **218**, 583.
3 J. Stubbe, *Adv. Enzymol.*, 1989, **63**, 349.
4 P. Nordlund and H. Eklund, *J. Mol. Biol.*, 1993, **232**, 123.
5 J. D. Lipscomb, *Annu. Rev. Microbiol.*, 1994, **48**, 371.
6 A. C. Rosenzweig, C. A. Frederick, S. J. Lippard and P. Nordlund, *Nature* (*London*), 1993, **366**, 537.
7 A. C. Rosenzweig, P. Nordlund, P. M. Takahara, C. A. Frederick and S. J. Lippard, *Chem. Biol.*, 1995, **2**, 409.
8 J. H. Satcher, Jr., M. W. Droege, T. J. R. Weakley and R. T. Taylor, *Inorg. Chem.*, 1995, **34**, 3317.
9 R. E. Stenkamp, L. C. Sieker and L. H. Jensen, *Acta Crystallogr.*, *Sect. B*, 1983, **39**, 697.
10 P. E. Clark and J. Webb, *Biochemistry*, 1981, **20**, 4628.
11 J. Ai, J. A. Broadwater, T. M. Loehr, J. Sanders-Loehr and B. G. Fox, *JBIC*, 1997, **2**, 37.
12 T. J. Mizoguchi and S. J. Lippard, *Inorg. Chem.*, 1997, **36**, 4526.
13 J. H. Satcher, Jr., A. L. Balch, M. M. Olmstead and M. W. Droege, *Inorg. Chem.*, 1996, **35**, 1749.
14 V. McKee, M. Zvagulis, J. V. Dagdigian, M. G. Patch and C. A Reed, *J. Am. Chem. Soc.*, 1984, **106**, 4765.
15 T.-Y. Dong, C. H. Huang, C. K. Chang, Y. S. Wen, L. S. Lee, J. A. Chen, W. Y. Yeh and A. Yeh, *J. Am. Chem. Soc.*, 1993, **115**, 6357.
16 G. M. Sheldrick, SHELXTL PLUS, Program Package for Structure Solution and Refinement, Siemens Analytical Instruments, Madison, WI, 1990.
17 G. M. Sheldrick, SHELXL 93, Program for Crystal Structure Refinement, University of Göttingen, 1993.
18 T. Sakurai, H. Kaji and A. Nakahara, *Inorg. Chim. Acta*, 1982, **67**, 1.
19 Y. Nishida, M. Takeuchi, H. Shimo and S. Kida, *Inorg. Chim. Acta*, 1984, **96**, 115.
20 P. Mathur, M. Crowder and G. C. Dismukes, *J. Am. Chem. Soc.*, 1987, **109**, 5227.
21 B. Bremer, K. Schepers, P Fleischhauer, W. Haase, G. Henkel and B. Krebs, *J. Chem. Soc.*, *Chem. Commun.*, 1991, 510.
22 Q. Chen, J. B. Lynch, P. Gomez-Romero, A. Ben-Hussein, G. B. Jameson, C. J. O'Connor and L. Que, Jr., *Inorg. Chem.*, 1988, **27**, 2673.
23 B. Eulering, F. Ahlers, F. Zippel, M. Schmidt, H.-F. Nolting and B. Krebs, *J. Chem. Soc.*, *Chem. Commun.*, 1995, 1305.
24 Y. H. Dong, S. P. Yan, V. G. Young, Jr. and L. Que, Jr., *Angew. Chem.*, *Int. Ed. Engl.*, 1996, **35**, 6618.
25 A. L. Feig, M. T. Bautista and S. J. Lippard, *Inorg. Chem.*, 1996, **35**, 6892.
26 C. K. Johnson, ORTEP, Report ORNL-5138, Oak Ridge National Laboratory, Oak Ridge, TN, 1976.
27 A. J. Bard and L. R. Faulkner, *Electrochemical Methods*, Wiley, New York, 1980.
28 T. F. Tekut, C. J. O'Connor and R. A. Holwerda, *Inorg. Chem.*, 1993, **32**, 324.
29 T. C. Gibb and N. N. Greenwood, *Mössbauer Spectroscopy*, Chapman and Hall, London, 1971, p. 148.
30 S. M. Gorun and S. J. Lippard, *Inorg. Chem.*, 1991, **30**, 1625.
31 J. M. McCormick, R. C. Reem and E. I. Solomon, *J. Am. Chem. Soc.*, 1991, **113**, 9066.

Paper 9/01905G